2009 Third International Conference on Quantum, Nano and Micro Technologies

Micromotor of Less Than 1 mm^3 Volume for In Vivo Medical Procedures

Brett Watson James Friend Leslie Yeo
Monash University
Dept. of Mechanical Engineering
Micro/Nanophysics Research Laboratory
Clayton, Victoria, 3800, Australia
Brett.Watson@eng.monash.edu.au

Abstract

The body's stress response to surgery has been cited as a primary cause of post-operative morbidity and has prompted growth in minimally invasive surgical techniques. The future of such techniques lies in the use of in vivo procedures, but is currently limited by the availability of motors with a volume of less than 1 mm^3.

In response to this we present a piezoelectric ultrasonic resonant micromotor with a volume of approximately 0.75 mm^3. The motor has a novel helically cut stator that couples axial and torsional resonant frequencies, excited by a lead zirconate titanate element 0.03 mm^3 in volume. The motor performance reaches a start-up torque of 47 nNm and no load angular velocity of 830 rad/s. This gives the motor a power density of 18.4 kW/m^3. This performance is on the order necessary to propel a swimming microbot in small human arteries.

1. Introduction

The body's stress response to surgery has been cited as a primary cause of post-operative morbidity and complications during post-operative care [14], which has led researchers to search for methods to reduce the stress caused by major surgical traumas [14],[3]. A successful method has been the use of minimally invasive surgery (MIS), which has been shown to reduce the stress caused by major procedures, and has led to new techniques in every speciality of surgical medicine [6].

Currently, catheters and endoscopes are the instruments most widely used during MIS. The instruments are introduced to the body by the surgeon, and require a high level of skill to control [8]. Despite the advances made and successes achieved with these instruments, in many circumstances MIS is not considered to be better than traditional cut and sew techniques. In such circumstances, current minimally invasive techniques are seen to lead to a loss of dexterity, feel and a compromised view of the procedure, even in the most complex and expensive systems [9].

To rectify this, research is being carried out on systems that will permit procedures to be conducted on the microscale using remotely operated micro-robots (microbots). Medical procedures using these devices will require only a small, or possibly no, incision in the body and will permit in vivo techniques to be used. The ultimate aim of such in vivo microbots is to carry out complex tasks including observation, sampling, drug delivery and surgical procedures within the cardiovascular, digestive and lymphatic systems [2].

To work effectively inside the human body, these microbots must be sub-millimetre in size, be able to move rapidly and accurately and conduct procedures with low power consumption. One of the major obstacles to realising such designs is the availability of a practical micromotor with a volume of less than 1 mm^3 to act as a drive system. Numerous methods have been proposed to realise the goal of a motor with a volume of less than 1 mm^3, the most successful of which include electrostatic [20], electromagnetic [12] and piezoelectric ultrasonic resonant [13] designs. If we examine the driving force used as the basis of design of these motors (electrostatic force, electromagnetic force and the converse piezoelectric effect), we can demonstrate that piezoelectric ultrasonic resonant motors have favourable scaling characteristics [18], high torque low speed outputs and simple construction, leading to the best potential for use as a practical micro-motor.

Some small scale piezoelectric ultrasonic resonant motors have been produced [13, 19], but due to a range of shortcomings common to current piezoelectric ultrasonic resonant designs, a rotational motor with a volume of significantly less than 1 mm^3 has not been achieved. Such shortcomings include the fragility of the motor due to the stator being fabricated from a piezoelectric ceramic, the in-

978-0-7695-3524-1/09 $25.00 © 2009 IEEE
DOI 10.1109/ICQNM.2009.14

creased motor complexity arising from requiring multiple electrical input signals and difficulties in fabrication. With a novel stator design, we have been able to simplify current piezoelectric ultrasonic resonant actuators, overcoming many of these shortcomings.

2. Basis of Operation

Piezoelectric ultrasonic resonant motors make use of the displacement associated with the excitation of a resonant mode or coupled modes within the motor stator. The carefully selected modes result in an elliptical cyclic motion at the point of contact between the stator and rotor (the stator tip). In conjunction with a friction coupling [16], this ensures a larger angular displacement is imparted on the rotor during one half of the vibration cycle, resulting in a net angular displacement after a complete cycle. The resonant mode(s) of the stator are excited by a harmonic loading from a piezoelectric element, arising from the converse piezoelectric effect.

Research to date has focussed on the use of coupled orthogonal bending modes to elicit elliptical motion at the stator tip [13, 19]. In general, bending modes are excited through the application of two electrical driving signals to a stator fabricated from a piezoelectric material. This results in the shortcomings outlined in Section 1.

For the motor design detailed in this paper, we use coupled axial and torsional resonant modes in place of the orthogonal bending modes. The coupled axial and torsional modes are to be excited by a lead zirconate titanate (PZT) piezoelectric element external to the stator. Fig. 1 demonstrates how the combination of the coupled mode shapes and the phase difference between the axial and torsional components, produces the desired elliptical motion at the stator tip. This methodology allows us to simplify the overall motor which has the following benefits:

• Reduced complexity – By coupling the axial and torsional resonant modes through the stator geometry, only one driving signal is required to run the motor.

• More robust – The piezoelectric element in the design is not part of the stator. This reduce the proportion of the motor that is fabricated from a piezoelectric ceramic, improving the robustness of the design.

• Improved fabrication – The piezoelectric element required is only a simple rectangular prism, making for easier fabrication. Other parts are fabricated by laser micromachining, a method common in micro-stent and surgical implant fabrication.

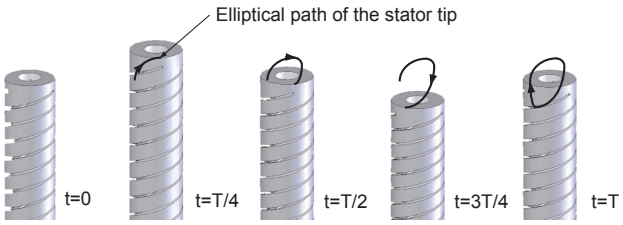

Figure 1. The axial and torsional resonant modes are coupled through the introduction of helical cuts to the stator. The coupled modes result in the elliptical stator tip motion as shown for one complete vibration cycle. Note: t is time and T is period.

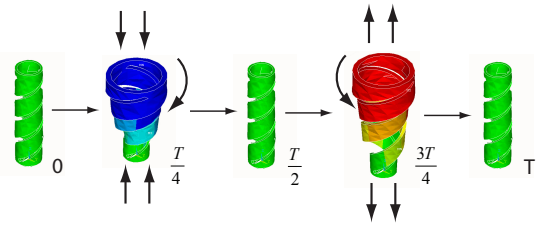

Figure 2. The exaggerated ANSYS output confirming the motion of the stator during one cycle of period T.

3 DESIGN AND FABRICATION

An initial helix angle of 30° was chosen based on the study by Wajchman et al. [17]. The study investigated the helix angle of a "twisted beam" and its effect on the coupling of axial and torsional resonance modes. A limited parametric study on the proposed stator geometry was carried out using the finite element analysis program ANSYS V10.0 (ANSYS Inc., Canonsburg, PA, USA). This study included the cut width, cut length and number of cuts (helix starts), and confirmed the elliptical stator tip motion. The exaggerated ANSYS output highlights the coupling of the axial and torsional motion as shown in Fig. 2. The finite element analysis also showed that using a helix angle of 30 ° lead to a stator design that had only weakly coupled axial and torsional resonant modes, with the axial resonant frequency approximately 30% higher than the equivalent torsional harmonic.

We hypothesise that a design that more closely matches the resonant modes would improve the motor performance. By focusing the parametric study on the number of helix revolutions (the helix angle) it was possible to determine

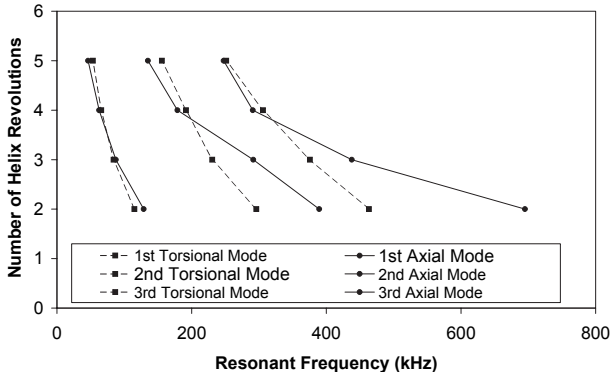

Figure 3. The axial and torsional resonant frequencies for the first three harmonics for a stator with three helical cuts and varying helix revolutions. The intersection of the curves identifies a stator geometry that closely matches the axial and torsional resonances.

stator geometries that more closely matched the axial and torsional resonant frequencies. Fig 3 is an extract from this study, demonstrating how the axial and torsional resonant frequencies vary with the number of revolutions in the helical cut. The intersection of the curves identifies a geometry that closely matches the torsional and axial resonant frequencies.

From the study, a stator geometry using 3.5 helix revolutions and three identical helical cuts was selected; Fig. 4 details the geometry dimensions. The motor prototype was fabricated from a 304 stainless steel tube with the helical cuts laser cut at equal circumferential spacing (fabricated by Laser Micromachining Solutions, Macquarie University, NSW, Aust.). A magnetic preload was used as part of the friction coupling, and was measured to be 53 μN. The resonant modes were excited by a 0.25 mm x 0.25 mm x 0.5 mm lead zirconate titanate (PZT) element (C203, Fuji Ceramics, Tokyo, Japan). The motor setup is shown in Fig. 5. The motor was trialled for each of the finite element model derived axial/torsional coupled resonant frequencies using a bandwidth of 5% to allow for manufacturing tolerances. The motor demonstrated bi-directional operation with clockwise rotation at the third harmonic, 732 kHz and counterclockwise rotation at the second harmonic, 526 kHz.

To confirm the study results, the ANSYS model was validated using a modified version of the method outlined by Friend et al. [4]. To experimentally determine the resonant modes, this method compares laser doppler vibrometer (LDV) measured displacement spectra at six points on the stator tip. With sensible application, this method allows the resonant modes to be classified directly from these spectra. These results are then compared with those produced by ANSYS. Fig. 6 shows the recorded spectra and comparable ANSYS results for a stator with five helix rotations and two cuts.

Object	Dimension (μm)
Base Tube	
Inside Diameter	200
Outside Diameter	241
Length	985
Helical Cut	
Width	28
Pitch	440
Length	880

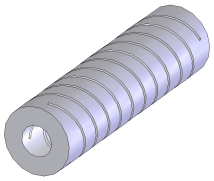

Figure 4. The stator geometry chosen to closely match the axial and torsional resonant frequencies while ensuring the overall volume remained less than 0.25 mm^3.

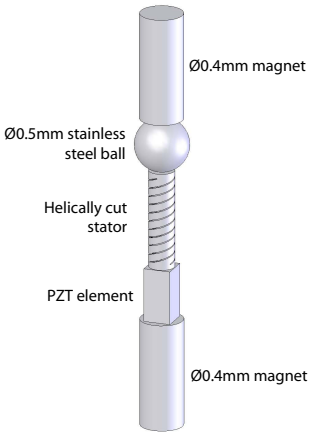

Figure 5. The motor set-up included the helically cut 240 μm diameter stator, a 0.5 mm diameter stainless ball as the rotor, a 0.25 mm x 0.25 mm x 0.5 mm PZT element, and two 0.4 mm diameter magnets to provide preload, resulting in a motor with a volume of less than 1 mm^3.

4 Results

Motor performance was determined using the method by Nakamura et al. [15]. Rotor motion was recorded using a laser doppler velocimeter (Canon LV-20Z, Kiyohara-Kogyodanchi, Utsunomiya-shi, Tochigi-ken, Japan). A maximum clockwise angular velocity of 830 rad/s (7,925 rpm) was recorded at an input of 20 V_{p-p} and 732 kHz. Based on the curve in Fig. 7, the average clock-

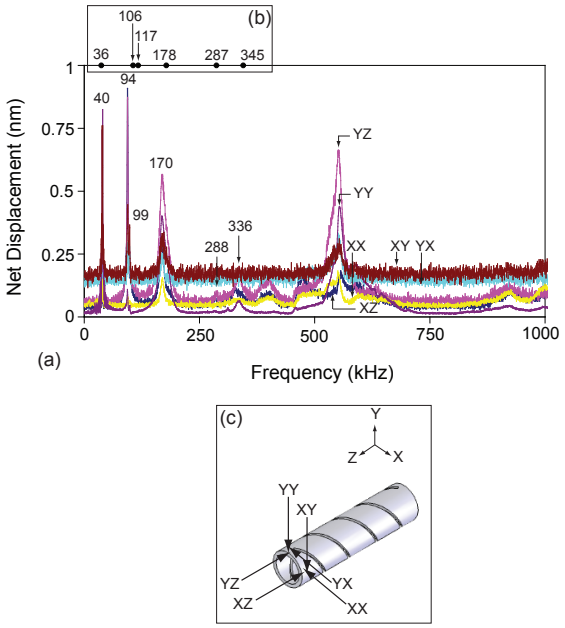

Figure 6. Finite element analysis validation through the comparison of stator resonant frequencies obtained from (a) LDV recorded displacement spectra and (b) ANSYS calculated frequencies using the measurement positions detailed in (c) for a stator with five helix revolutions and two helical cuts.

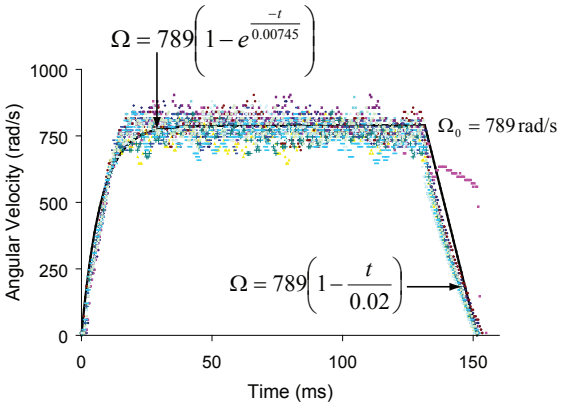

Figure 7. The angular velocity vs. time curve, as derived by the method in [15], for an applied step voltage of 20 V_{p-p}, preload of 53 μN and an operating frequency of 732 kHz. The fitted curve is average obtained across all runs as recorded by the points.

wise start-up torque was 47 nNm with a peak of 51 nNm and a minimum of 39.8 nNm. The fitted exponential curve is derived from the standard curve for a piezoelectric ultrasonic motor [15]. The average braking torque was calculated to be 17.8 nNm. A maximum counterclockwise angular velocity of 1600 rad/s (15,280 rpm) at 32.1 Vp-p and 526 kHz was recorded; however, the inconsistent nature of the operation prevented the measurement of the complete motor performance.

5 Discussion

The reported motor demonstrated bidirectional operation, however, counterclockwise motion was unreliable when compared with clockwise operation. When making use of two sequential torsional modes to obtain bidirectional motion, as is the case here, we expect the clockwise direction to be superior due to the tendency of the stator to "uncurl" in that direction during extension of the stator. This is a result of the helical geometries used in the design and will benefit the performance of the motor through an increased tangential displacement for each cycle. By matching the desired operational frequencies of the motor to the resonant mode of the piezoelectric element we will ensure the maximum motor performance, which will enable a consistent bi-directional operation to be achieved. Further research into the exact geometry mechanisms driving the changes in the axial/torsional resonant frequencies is required to realise the successful matching of piezoelectric and stator resonant modes.

We now give an example of how such a motor may be used for in vivo medical procedures. We examine a "swimming microbot" that uses an E.coli-like flagella as a means of propulsion. Such microbots have been highlighted as having great potential for use in in vivo medical procedures due to the low Reynolds number propulsion system [1]. We use Higdon's model for flagellar propulsion [11], to determine the average power required for swimming in small human arteries:

$$\bar{P} = 6\pi\mu A\bar{U}^2\eta_0^{-1}K$$

where blood has a viscosity of approximately μ =0.004 Pa-s [7]; A, is the radius of the swimming microbot which we assume to be approximately the size of the motor, 150 μm, K is the Stokes' law correction for a prolate spheroid, 2.7 [10], and $\eta_0^{-1} = 200$ from Higdon's results. For useful operation, the device should at least swim as fast as the blood flow, in the case of the right central retinal artery—a suitable example of a location both difficult to reach by other means and presumably one where this device would be used—$\bar{U} \approx 6.0$ cm/s [5], giving a required input power of 24 μW.

The average power output of the motor is approximately

$(\phi_{max}T_{max})/4 = 9.75\ \mu$W, where ϕ_{max} is the maximum clockwise velocity and T_{max} is the average start-up torque. Although this power is smaller than what is required, it is potentially not out of reach of such a device.

6 Conclusion and Future Work

We have demonstrated a motor with potential applications in in vivo medical procedures. The novel stator design coupling axial and torsional resonant modes simplifies current piezoelectric ultrasonic resonant designs and results in a motor volume of less than 1 mm^3. The motor has a peak torque of 51 nNm and a maximum rotational velocity in excess of 15,000 rpm. The motor performance was theoretically shown to be significant enough to propel a swimming microbot in the human body.

Future work on this design will focus on two areas; improved performance and reliability, and applications. To improve the performance of the motor, further research will be conducted to develop an analytical model of the motor. This model will act as a design tool to allow the axial and torsional stator resonances to be more closely matched to the thickness resonance of the piezoelectric element. This is expected to improve the motor performce and produce stable bi-directional operation. Research will also be conducted into creating a more reliable and compact rotor/preload arrangement, ensuring the motor is ready to be used in a range of applications. Of a main interest in application trials will be to trial the motor in conjucntion with a flagella propulsion system, confirming the throetical prediction outlined in Section 5.

References

[1] B. Behkam and M. Sitti. Design methodology for biomimetic propulsion of miniature swimming robots. *ASME Journal of Dynamic Systems and Measurement Control*, 128:36–43, 2006.

[2] F. Cepolina, B. Challacombe, and R. Michelini. Trends in robotic surgery. *Journal of Endourology*, 19(8):940–951, 2005.

[3] J. Desborough. The stress response to trauma and surgery. *British Journal of Anaesthesia*, 85(1):109–117, 2000.

[4] J. Friend, K. Nakamura, and S. Ueha. A torsional transducer through in-plane shearing of paired planar piezoelectric elements. *IEEE Transactions on Ultrasonics, Ferroelectrics, and Frequency Control*, 51(7):870–877, 2004.

[5] G. Fuchsjger-Mayrl, K. Polak, A. Luksch, E. Polska, G. Dorner, G. Rainer, H.-G. Eichler, and L. Schmetterer. Retinal blood flow and systemic blood pressure in healthy young subjects. *Graefe's Archive for Clinical and Experimental Ophthalmology*, 239(9):673–677, 2001.

[6] K. Fuschs. Minimally invasive surgery. *Endoscopy*, 34:154–159, 2002.

[7] J. Galduróza, H. Antunesb, and R. Santos. Gender- and age-related variations in blood viscosity in normal volunteers: A study of the effects of extract of allium sativum and ginkgo biloba. *Phytomedicine*, 14:447–451, 2007.

[8] Y. Haga and M. Esashi. Biomedical microsystems for minimally invasive diagnosis and treatment. *Proceedings of the IEEE*, 92(1):98–114, 2004.

[9] E. Hanly and M. Talamini. Robotic abdominal surgery. *The American Journal of Surgery*, 188:19S–26S, October 2004.

[10] J. Happel and H.Brenner. *Low Reynolds Number Hydrodynamics*. Prentice Hall, Englewood Cliffs, NJ, 1965.

[11] J. Higdon. The hydrodynamics of flagellar propulsion: Helical waves. *Journal of Fluid Mechanics*, 94:331–351, 1978.

[12] K. Hori, T. Miyagawa, and K. Ito. Development of ultra-small sized servo actuator with brushless DC motor, planetary gear drive and optical rotary encoder. *International Journal of the Japan Society for Precision Engineering*, 31:1–5, 1997.

[13] T. Kanda, A. Makino, L. Suzumori, T. Morita, and M. Kurosawa. A cylindrical micro ultrasonic motor using a micromachined bulk piezoelectric transducer. In *IEEE Ultrasonics Symposium*, 2004.

[14] H. Kehlet and D. W. Wilmore. Fast-track surgery. *British Journal of Surgery*, 92(1):3–4, 2005.

[15] M. Nakamura, K.and Kurosawa and S. Ueha. Characteristics of a hybrid transducer-type ultrasonic motor. *IEEE Transactions on Ultrasonics, Ferroelectrics, and Frequency Control*, 38(3):6, 1991.

[16] K. Uchino. Piezoelectric ultrasonic motors: Overview. *Smart Material Structures*, 7:273–285, 1998.

[17] D. Wajchman, D. Liu, J. Friend, and L. Yeo. An ultrasonic piezoelectric motor utilising a non-circular cross sectioned twisted beam. *IEEE Transactions on Ultrasonics, Ferroelectrics and Frequency Control*, 55(4):832–840, 2008.

[18] Z. Wang. Nanopiezotronics. *Advanced Materials*, 19:889–892, 2007.

[19] H. Zhang, S. Dong, S. Zhang, T. Wang, Z. Zhang, and L. Fan. Ultrasonic micro-motor using miniature piezoelectric tube with diameter of 1.0 mm. *Ultrasonics*, 44:e603–e606, 2006.

[20] W. Zhang, G. Meng, and H. Li. Electrostatic micromotor and its reliability. *Microelectronics Reliability*, 45:1230–1242, 2005.